CrystEngComm

View Online
Dynamic Article Links

Cite this: DOI: 10.1039/c1ce05705g

www.rsc.org/crystengcomm

PAPER

Facile synthesis of zinc(II)-carboxylate coordination polymer particles and their luminescent, biocompatible and antibacterial properties†

Kuaibing Wang, Yuxin Yin, Chengying Li, Zhirong Geng and Zhilin Wang*

Received 9th June 2011, Accepted 14th July 2011
DOI: 10.1039/c1ce05705g

Four different morphologies, including 1D nanobelts (**1**), 3D nanorod-flowers (**2**), fan-like (**3**) and rhombus-like (**4**) architectures have been synthesized from the mild reaction of $Zn(Ac)_2 \cdot 2H_2O$ and 2,2′-bipyridine-4,4′-dicarboxylic acid (H_2L). The shape of the resulting coordination polymer particles (CPPs) was dependent on the amount of solvent and the molar ratio of reactants used in the reaction. In the experimental process, some additives such as triethylamine and acetic acid played a vital role in the formation of CPPs as means of adjusting the deprotonation rate of the organic linker (H_2L), and thus affected the morphology of the resulting CPPs. We also investigated the effect of the different morphologies on the luminescent properties and bioactivities.

1. Introduction

Zinc-based coordination polymer particles (Zn-CPPs) are of great importance currently due to their useful applications such as in ion exchange,[1] gas storage[2] and explosive sensors.[3] With the development of nanoscience and nanotechnology, several preparation methods of micro- and nano-sized particles made from coordination polymers have been reported by several research groups.[4–6] However, these methods for controlling particle size and shape are still fairly rudimentary.[7] Just as the chemical and physical properties of inorganic particles (metal, metal alloy, or quantum dot) can be affected by the size and shape, presumably so too does the size and morphology of CPPs influence their own properties and applications. However, thus far, much more attention has been devoted to studying the morphologies effect on the gas-sorption properties due to their different surface areas, and to the best of our knowledge, only a few reports have been concerned about other applications as a function of their micro/nanoscale architectures.[8] One of the reasons for this phenomenon is that it is challenging to characterize their structures, which therefore creates a constant challenge for researchers, to design programs for correlating structure and function of CPPs. Indeed, many CPPs in the literature don't report their structures and thus restrict their extensive applications.[9]

Recent studies indicate that many inorganic nanomaterials have shown severe toxicity, which may impose restrictions on a range of medical and environmental applications.[10,11] In contrast with inorganic nanomaterials, the nanoparticles of coordination polymers have been designed as ideal candidates for a new valuable solution in the field of drug-delivery systems because of their biocompatibility and biodegradability.[12,13] Thus, investigating the biocompatible nature of CPPs is of great importance. It is noteworthy that nanomaterials possess high antibaterial activity with minimal perturbation to human cells, which can be used in the medical and environmental field.[14–16] So far, a significant antibacterial activity can be induced for coordination polymers by using either a biocation or a metal ion exhibiting inhibitory properties.[17] Herein, we report the preparation of micro- and nano-sized Zn-CPPs with four different shapes, including 1D nanobelts (**1**), 3D nanorod-flowers (**2**), fan-like (**3**) and rhombus-like (**4**) architectures from the mild reaction of zinc(II) metal ions with 2,2′-bipyridine-4,4′-dicarboxylic acid (H_2L), and we investigated their bioactivities. In this article, the crystal structure was also studied to characterize the structure of the as-synthesized nanomaterial. The results show that the four as-synthesized CPPs are isostructural. In addition, the influence of the molar ratio of reactant, and additives such as triethylamine and acetic acid on the morphology of resulting CPPs will also be documented.

State Key Laboratory of Coordination Chemistry, Coordination Chemistry Institute, Nanjing National Laboratory of Microstructures, Nanjing University, Nanjing, 210093, P. R. China. E-mail: wangzl@nju.edu.cn

† Electronic supplementary information (ESI) available: Fig. SI1–SI4 showing EDX spectra, TGA curve of one of the CPPs, SEM images of rhombus-like particles and the possible growth mechanism of nanobelts and nanorod-flower. CCDC reference number 798766. For ESI and crystallographic data in CIF or other electronic format see DOI: 10.1039/c1ce05705g

2. Experimental

Preparation of coordination polymer particles

First, $Zn(Ac)_2 \cdot 2H_2O$ (0.224 g) was dissolved in 200 mL H_2O/CH_3CH_2OH (v : v, 1 : 1) to form a clear solution. Then, under vigorous magnetic stirring, (i) in the presence of HAc additive (1 mL), $Zn(Ac)_2 \cdot 2H_2O$ (15 mL) and H_2L (0.012 g) with a molar

ratio about 3 : 2 was added in (5 mL or 20 mL) water, the reaction was kept at room temperature (RT) for 2 h, and nanobelts and nanorod-flower particles were formed, respectively. (ii) In the presence or absence of Et_3N additive (50 μL), $Zn(Ac)_2 \cdot 2H_2O$ (10 mL) and H_2L (0.012 g) with a molar ratio about 1 : 1 was added in 30 mL mixed solvents of water and ethanol (v : v, 1 : 1), the reaction was kept at RT for 4 h, and fan-like and rhombus-like particles were obtained, respectively. Then these solid materials were collected by centrifugation and washed with water and ethanol three times. IR for **1** (KBr pellet, cm^{-1}): 3384 (s), 1607 (s), 1555 (s), 1385 (s), 1259 (m), 1113 (w), 1037 (w), 860 (w), 786 (m), 701 (m). Anal. calc. for **1**: C, 34.67; H, 4.36; N, 6.74%. Found: C, 34.53; H, 4.42; N, 6.71%. IR for **2** (KBr pellet, cm^{-1}): 3312 (s), 1617 (s), 1532 (s), 1388 (s), 1280 (m), 1259 (m), 1039 (m), 858 (w), 776 (m), 692 (m). Anal. calc. for **2**: C, 34.67; H, 4.36; N, 6.74%. Found: C, 34.73; H, 4.32; N, 6.68%. IR for **3** (KBr pellet, cm^{-1}): 3375 (s), 1607 (s), 1564 (s), 1396 (s), 1301 (m), 1227 (m), 1137 (w), 1007 (m), 860 (w), 786 (m), 692 (m). Anal. calc. for **3**: C, 34.67; H, 4.36; N, 6.74%. Found: C, 34.69; H, 4.39; N, 6.77%. IR for **4** (KBr pellet, cm^{-1}): 3370 (s), 1617 (s), 1535 (s), 1396 (s), 1291 (m), 1248 (m), 1028 (m), 848 (w), 786 (m), 696 (m). Anal. calc. for **4**: C, 34.67; H, 4.36; N, 6.74%. Found: C, 34.74; H, 4.23; N, 6.65%.

Preparation of bulk-crystals

The crystals were prepared by a layering method. A solution of H_2L (0.012 g, 0.05 mmol) in water (5 mL) was adjusted to pH = 7 using 0.5 mol L^{-1} NaOH aqueous solution at room temperature. A buffer layer of a solution (8 mL) of ethanol and water (1 : 1) was carefully layered over the aqueous solution, and then a solution (4 mL) of $Zn(Ac)_2 \cdot 2H_2O$ (0.011 g, 0.05 mmol) in ethanol and water (4 : 1) was layered over the buffer layer. The bulk-crystals were collected after several weeks. IR (KBr pellet, cm^{-1}): 3217 (s), 1637 (s), 1543 (s), 1376 (s), 1280 (m), 1239 (m), 1028 (w), 870 (w), 765 (m), 687 (m). Anal. calc. for $C_{12}H_{18}N_2O_{10}Zn$: C, 34.67; H, 4.36; N, 6.74%. Found: C, 34.62; H, 4.30; N, 6.78%.

MTT proliferation assay

HepG2 cells were grown in RPMI 1640 medium supplemented with 10% freshly inactivated fetal calf serum (FCS) and were seeded equivalently into a 96-well plate; the concentrations of as-synthesized samples were 30 μg mL^{-1}. The plates were kept at 37 °C in a humidified atmosphere of 5% CO_2 and incubated for 12, 24 and 48 h; then MTT solution of an appropriate concentration (1 mg mL^{-1}) was added to each well and the plates were incubated at 37 °C for 4 h. The measurements of absorbance of the solutions relating to the number of live cells were performed on an ELISA spectrophotometer at 570 nm.

Antibacterial test

The antibacterial activity of the synthesized CPPs was tested against *B. subtilis*, *S. aureus*, *S. enteriditis*, *E. coli*, *P. vulgaris* and *P. aeruginosa* by determining the minimum inhibitory concentrations (MICs, μg mL^{-1}) through a colorimetric method using the dye MTT (3-(4,5-dimethylthiazol-2-yl)-2,5-diphenyltetrazolium bromide). Firstly, the stock solution of the synthesized samples (50 μg ml^{-1}) were prepared in dimethyl sulfoxide (DMSO) and graded quantities of the test crystals were incorporated in specified quantities of sterilized liquid medium. Secondly, the solutions were poured into microtitration plates, and then a suspension of the microorganism with concentration approximately 10^5 cfu mL^{-1} was added. After incubation at 37 °C for 24 h, 50 μL of PBS (phosphate buffered saline, 0.01 mol L^{-1}, pH 7.4: $Na_2HPO_4 \cdot 12H_2O$ 2.9 g, KH_2PO_4 0.2 g, NaCl 8.0 g, KCl 0.2 g, distilled water 1000 mL) containing 2 mg mL^{-1} of MTT was added to each well. Incubation was continued at room temperature for 4–5 h, followed by the addition of 100 μL of isopropanol containing 5% 1 mol L^{-1} HCl to extract the dye. The optical density (OD) was measured with a microplate reader at 570 nm to determine the MICs.

General methods

Elemental analyses of C, H, and N were performed on an Elementar Vario MICRO Elemental Analyzer at the Analysis Centre of Nanjing University. Fourier-transformed infrared (FT-IR) spectra were obtained on a Bruker Vector 22 FT-IR spectrophotometer using KBr pellets. Thermogravimetrical and differential thermal analyses (TG-DTA) were performed in a N_2 atmosphere (a flow rate of 100 mL min^{-1}) on a simultaneous SDT 2960 thermal analyzer from 35 °C up to 600 °C, with a heating rate of 10 °C min^{-1}. X-ray powder diffraction (XRPD) data were collected on a Bruker D8 Advance instrument using Cu-Kα radiation (λ = 1.54056 Å) at room temperature. The morphology of the as-prepared samples and the corresponding energy dispersive X-ray (EDX) spectroscopy were obtained using a Hitachi S-4800 field-emission scanning electron microscope (FE-SEM). X-Ray crystallographic data of bulk-crystals were collected on a Bruker Apex Smart CCD diffractometer with graphite-monochromated Mo-Kα radiation ($\lambda = 0.71073$ Å). All non-hydrogen atoms were refined anisotropically by the full-matrix least-squares method on F^2. The structure was solved by direct methods and refined using the SHELXL-97 program package.[18,19] The crytallographic data for bulk-crystals is depicted in Table 1.

3. Results and discussion

The structures of all the coordination polymer species (**1**)–(**4**) are supported by X-ray powder diffraction (XRD) results as shown in Fig. 1. The diffraction of these polymers can be readily indexed to the bulk-crystals which have been synthesized by a layer method at room temperature. The results suggest that the as-synthesized species are isostructural with the bulk-crystals.

The crystal structure is illustrated in Fig. 2, each organic linker (H_2L) bridged two metal ions to form a 1D metal–carboxylate chain, and then these zigzag-like chains are parallel to each other and pack in ABAB mode to give rise to a 2D network with the aid of hydrogen bonds. The same chemical composition of (**1**)–(**4**) was also confirmed by elemental analysis (EA) and infrared spectroscopy (IR) and energy dispersive X-ray (EDX) spectroscopy (Fig. SI1 in the ESI†). The CO stretching frequency at 1695 cm^{-1} for uncoordinated H_2L shifted to around 1607 cm^{-1}, illustrating the complete deprotonation of the carboxylate group after the formation of coordination polymers. In addition,

Table 1 Crystallographic data for bulk-crystals

	Bulk-crystals
Chemical formula	$C_{12}H_{18}ZnN_2O_{10}$
F_w	415.65
Cryst. size/mm	0.30 × 0.10 × 0.10
Cryst. syst.	Monoclinic
Space group	$P2_1/c$
T/K	291(2)
a/Å	7.1290(3)
b/Å	12.1480(12)
c/Å	17.7600(13)
α/°	90
β/°	101.580(3)
γ/°	90
V/Å^3	1506.8(2)
Z	4
D_c/g cm^{-3}	1.806
μ/mm^{-1}	1.691
Reflections collected/unique	7701/2963
Data/restraints/params	2963/0/226
R_{int}	0.0570
R_1, wR_2 [$I > 2\sigma(I)$]	0.0520, 0.1135
R_1, wR_2 (all data)	0.0672, 0.1169
GOF on F^2	1.067
F(000)	832

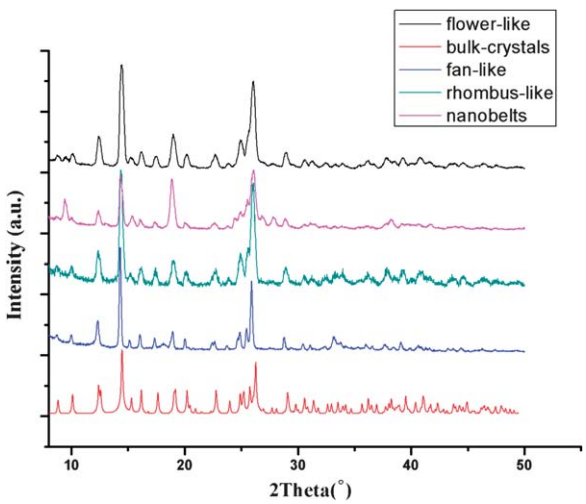

Fig. 1 XRD patterns of the bulk-crystals and the as-synthesized CPPs.

thermogravimetric analysis (TGA) can also show that as-synthesized CPPs were isostructural with bulk crystals; it revealed that the CPPs were stable up to 400 °C after an initial weight loss of 25% due to water liberation (coordination water and lattice water molecules) in the 50–100 °C temperature range (Fig. SI2 in the ESI†). EDX confirms that the resulting samples are composed of Zn, C, N and O, in agreement with the results of elemental analysis.

In the experimental process, in the presence of acetic acid (HAc) (Scheme 1), the solution of $Zn(Ac)_2 \cdot 2H_2O$ was reacted with the organic linker (H_2L) in the molar ration of 3 : 2 at RT, and 1D nanobelts were maintained as evidenced by the field-emission scanning electron microscopy (SEM) image in Fig. 3a–b, the average size of the width was determined by SEM to be 100 nm. Keeping the other reaction conditions unchanged, we

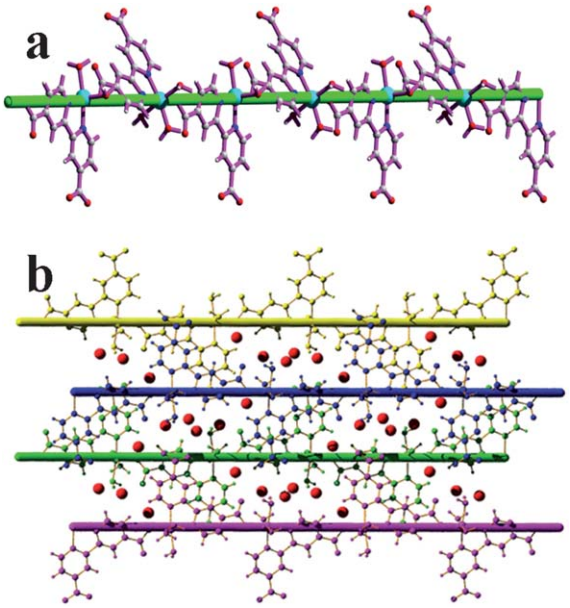

Fig. 2 (a) 1D zigzag-like metal–carboxylate chain viewed along the a axis. (b) Schematic drawing of 2D networks viewed along the a axis (the lattice water molecules in the channel were presented here by red balls).

increased the amount of water from 5 mL to 20 mL, and a 3D nanorod-flower morphology was obtained. Fig. 3c reveals the flower-like architectures are produced by many rod-like motifs. The diameter of each flower is about 5–7 μm, as seen in Fig. 3c. Fig. 3d displays a higher magnified SEM image which indicates that the width of the rods vary from 100 nm to 150 nm. The result reveals that the morphology generated has a strong positive correlation to the amount of solvent used. With lower concentrations of modulator, the nucleation occurs faster. A great number of nuclei can be obtained and rapidly grow at the same time, while the available reagents are quickly depleted, affording smaller crystals with homogeneous size distribution.[21] The possible reason for this phenomenon is that acetic acid is used to delay the deprotonation rate of the organic linker (H_2L) in the

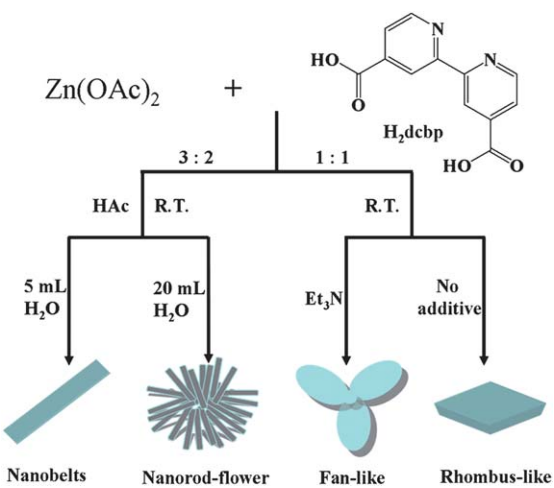

Scheme 1 Preparation of four different morphologies of coordination polymer particles.

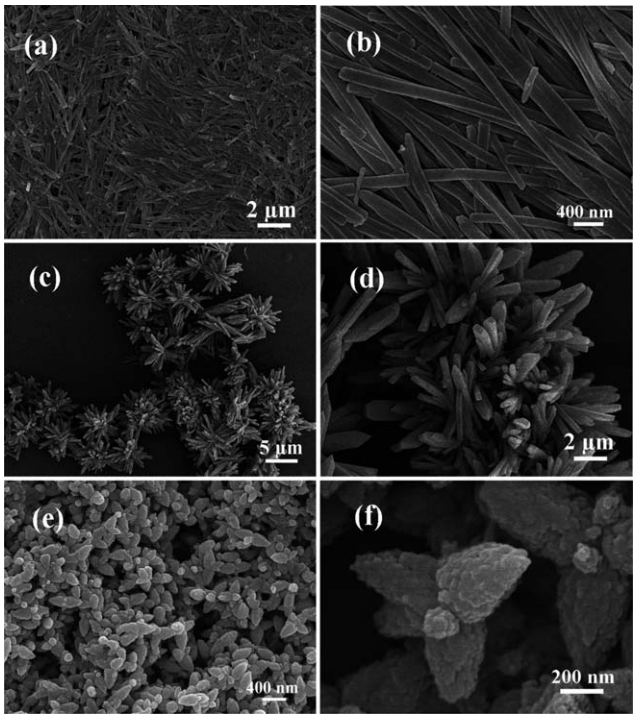

Fig. 3 (a)–(b) SEM images of nanobelt morphology. (c)–(d) SEM images of nanorod-flower morphology. (e)–(f) SEM images of fan-like morphology.

experimental process,[20] and the different concentration of acetic acid greatly influences the deprotonation rate and consequently the resulting morphology.[21] When acetic acid was added in the reaction system, as the amount of solvent increased, the concentration of HAc decreased, and thus the deprotonation rate of the building blocks resulting in nanrod-flower architectures is more rapid than that for nanobelts.

To control the shape of the products, we varied other reaction conditions and found that the additives and the molar ratio of reactants are important factors. In the presence of triethylamine (Et_3N), we varied the molar ratio of reactants from 3 : 2 to 1 : 1, fan-like CPPs were formed as shown in Fig. 3e–3f. It can be observed from Fig. 3f that the fan-like sample obtained was composed of three fan blades, the length and the width of each blade are about 500 nm and 300 nm, respectively. Another control experiment to figure out the role of Et_3N was performed in the absence of Et_3N, in this experiment, the rhombus-like CPPs were maintained on a large scale as depicted in Fig. SI3 in the ESI.† It can be observed clearly that the average size of rhombic particles is about 1.64 ± 0.44 μm. It is noteworthy that the basic Et_3N acts as a pH value controller to adjust the particle formation rate and thus the resulting particle shape. From these observations, we could conclude that the additives such as HAc and Et_3N play an important role in adjusting the formation rate of CPPs and eventually their particle morphology. In addition, the resulting particles were found to be stable in several solvents such as DMF, DMSO, methanol, pyridine and nonpolar solvents. On the basis of the above studies, a possible growth mechanism of 1D nanobelts and hierarchical nanrod-flowers is proposed as shown in Fig. SI4;† under high concentrations of

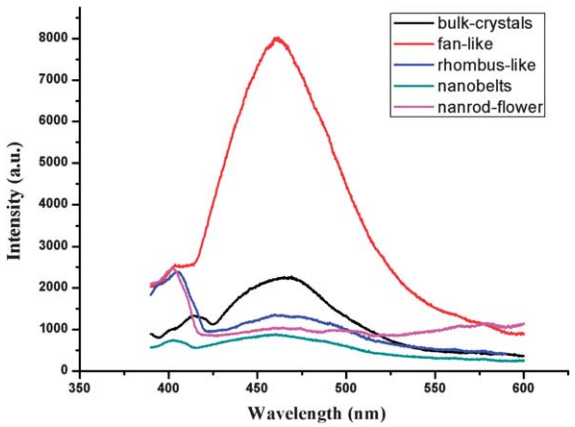

Fig. 4 Fluorescence spectra of solid bulk-crystals and CPPs of different morphologies at room temperature.

HAc additive,[21] HAc delays the deprotonation rate of the organic linker leading to few nucleation events. As the reaction continues, the numbers of Zn nuclei in combination with the constant merging of deprotonated organic linker leads to the slow arrangement of growing crystal seeds; after the aggregation of these crystal seeds, the nanobelt morphology was obtained under vigorous stirring. The mechanism for the formation of nanorod-flowers is close to that of nanobelts, the possible reason for forming different resulting morphologies may be due to the low concentration of HAc leading to fast nucleation.[21] The result confirms that the concentration of additive does greatly influence the resulting shape of nanoparticles.

The photoluminescence properties of (**1**)–(**4**) and bulk-crystals were studied in the solid state at RT upon excitation at 370 nm. As shown in Fig. 4, the resulting particles and bulk-crystals all exhibit blue luminescence emissions at 400 nm (weak) and 472 nm (strong). In comparison with the free organic ligand (a weak emission at 422 nm ($\lambda_{ex} = 372$ nm)),[22] the emissions of (**1**)–(**4**) may be attributable to ligand-to-metal charge transfer (LMCT) due to the blue shift of 50 nm.[23] It is obvious that the intensity of fan-like particles is the strongest in these CPPs,

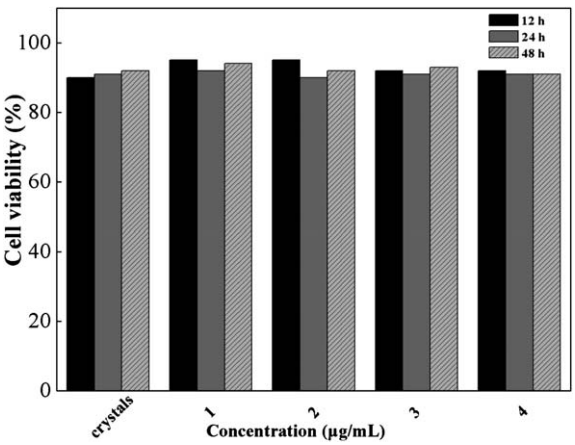

Fig. 5 The viabilities of HepG2 cells incubated with bulk-crystals and the as-synthesized samples at the same concentration for different time periods.

Table 2 MICs (minimum inhibitory concentrations) (μg mL^{-1}) of the organic ligand H_2dcbp and as-synthesized CPPs[a]

	Minimum inhibitory concentration/μg mL^{-1}					
	Gram positive		Gram negative			
Samples	*B. subtilis*	*S. aureus*	*S. enteriditis*	*E. coli*	*P. vulgaris*	*P. aeruginosa*
H_2dcbp	+	+	+	+	+	+
Nanobelts	>50	>50	>50	25	25	25
Nanorod-flowers	>50	>50	25	12.5	12.5	12.5
Fan-like structures	>50	25	>50	25	>50	12.5
Rhombus-like structures	>50	25	>50	25	>50	25
$[ZnCl_2(HATtsc)]\cdot CH_3CN$[33]	>100	>100	—	>100	—	>100
$[Zn(L)(H_2O)]Cl_2\cdot 3H_2O$[34]	50	—	—	50	50	—

[a] "+" means growth.

however, the peak shape of as-synthesized samples are the same as the one of bulk-crystals. These observations reveal that the morphologies of particles with identical structure do have effects on the luminescent intensities. The possible reason for the different enhancement of luminescence of synthesized CPPs may be attributed to the organic linker chelating to the metal center, which effectively increases the rigidity of the ligand, and the influence of different morphologies leads to different reduction of energy loss by nonradioactive decay.[24] The observed enhancement may be explained by the donor–acceptor electron-transfer mechanism.[25] Furthermore, the strongest intensity of fan-like particles may be due to their high surface area, which is easier to absorb the external excitation light and obtain the high bulk density, and thus reduce light scatter to enhance its luminescent intensity.[26,27]

Thus far, CPPs have been used for a wide range of applications in many fields, however, as far as we know, no literature has reported their bioactivities. The main requirement of implanted artificial materials or biomaterials, except their mechanical properties, is their biocompatibility.[28] Fig. 5 shows cell viabilities of HepG2 cells incubated with organic linker and as-synthesized particles under the same concentrations for different time periods. According to the results, the bioactivity of nanobelts was close to nanorod-flowers, while the biocompatibility of rhombic and fan-like particles was close to that of the bulk crystals. It can be seen that both the bulk crystals and as-synthesized species have good biocompatibility. In contrast with some traditional inorganic particles, such as titanium dioxide (TiO_2) and silicon dioxide (SiO_2), nanoparticles are not strictly envisioned for biomedical applications due to their potential toxicity.[29,30] In this regard, we also studied the antimicrobial activities of the resulting Zn-CPPs against *B. subtilis*, *S. aureus*, *S. enteriditis*, *E. coli*, *P. vulgaris* and *P. aeruginosa* by determining the minimum inhibitory concentrations (MIC, μg mL^{-1}) through a colorimetric method using the dye MTT.[31] The results are depicted in Table 2 and illustrate that fan-like particles can kill gram negative bacteria well; stronger than the other sample particles. Taking the ligand that has no effect on the antibacterial activity into consideration, the antibacterial activities of Zn-CPPs could be explained by using chelation theory according to reported literature.[32,33] The ligand coordinating to Zn ions tends to make the resulting CPPs act as more powerful and potent bactericidal agents, killing more of the bacteria than the ligand. It is notable that the morphology can influence the resulting antimicrobial activity. Although the real antibacterial mechanism is still uncertain, the reason for different antibacterial activities may be that nanorod-flower particles are assembled from lots of nanorods; these nanorods and their interior structure might effectively inhibit the growth of gram negative bacterial. When compared with the reported zinc complexes, the resulting samples have stronger antibacterial activities than the reported ones.[34,35]

4. Conclusions

In summary, the *O*,*N*-bifunctional organic ligand, 2,2′-bipyridine-4,4′-dicarboxylic acid (H_2L), has been documented for synthesizing CPPs with different morphologies which have an identical structure with bulk-crystals. Additives such as Et_3N and acetic acid play an important role in the particle formation rate by means of manipulating the deprotonation rate of the organic linker and thus in the particle size and shape. In addition, the as-synthesized CPPs have good bioactivities which may show potential uses in medical and environmental applications. This research also demonstrates that the morphologies do have effects on the luminescent properties and antibacterial activities.

Acknowledgements

This work was supported by the National Natural Science Foundation of China (21075064, 21027013, 21021062 and 90813020) and the National Basic Research Program of China (2007CB925102).

Notes and references

1 M. Oh and C. A. Mirkin, *Nature*, 2005, **438**, 651.
2 O. K. Farha, Y. M. Spokoyny, K. L. Mulfort, S. Galli, J. T. Hupp and C. A. Mirkin, *Small*, 2009, **5**, 1727.
3 C. Y. Zhang, Y. K. Che, Z. X. Zhang, X. M. Yang and L. Zang, *Chem. Commun.*, 2011, **47**, 2336.
4 Z. Ni and R. I. Masel, *J. Am. Chem. Soc.*, 2006, **128**, 12394.
5 W. Cho, Y. H. Lee, H. J. Lee and M. Oh, *Chem. Commun.*, 2009, 4756.
6 T. Tsuruoka, S. Furukawa, Y. Takashima, K. Yoshida, S. Isoda and S. Kitagawa, *Angew. Chem., Int. Ed.*, 2009, **48**, 1.
7 M. Oh and C. A. Mirkin, *Angew. Chem., Int. Ed.*, 2006, **45**, 5492.
8 D. Tanaka, A. Henke, K. Albrecht, M. Moeller, K. Nakagawa, S. Kitagawa and J. Groll, *Nat. Chem.*, 2010, **2**, 410.

9 S. Park, W. Cho and M. Oh, *CrystEngComm*, 2010, **12**, 1060.
10 W. Hu, C. Peng, W. Luo, M. Lv, X. Li, D. Li, Q. Huang and C. Fan, *ACS Nano*, 2010, **4**, 4317.
11 H. Pang, Q. Lu, Y. Li and F. Gao, *Chem. Commun.*, 2009, 7542.
12 P. Horcajada, T. Chalati, C. Serre, B. Gillet, C. Sebrie, T. Baati, J. F. Eubank, D. Heurtaux, P. Clayette, C. Kreuz, J.-S. Chang, Y. K. Hwang, V. Marsaud, P.-N. Bories, L. Cynober, S. Gil, G. Férey, P. Couvreur and R. Gref, *Nat. Mater.*, 2010, **9**, 172.
13 P. Horcajada, C. Serre, M. Vallet-Regí, M. Sebban, F. Taulelle and G. Férey, *Angew. Chem., Int. Ed.*, 2006, **45**, 5974.
14 Z. Guo and P. J. Sadler, *Angew. Chem., Int. Ed.*, 1999, **38**, 1512.
15 V. Alt, T. Bechert, P. Steinrücke, M. Wagener, P. Seidel, E. Dingeldein, E. Domann and R. Schnettler, *Biomaterials*, 2004, **25**, 4383.
16 A. Travan, C. Pelillo, I. Donati, E. Marsich, M. Benincasa, T. Scarpa, S. Semeraro, G. Turco, R. Gennaro and S. Paoletti, *Biomacromolecules*, 2009, **10**, 1429.
17 R. Olar, M. Badea, D. Marinescu, M.-C. Chifiriuc, C. Bleotu, M. N. Grecu, E.-E. Iorgulescu and V. Lazar, *Eur. J. Med. Chem.*, 2010, **45**, 3027.
18 G. M. Sheldrick, *SHELXS 97, Program for Crystal Structure Solution*, University of Göttingen, Göttingen, 1997.
19 G. M. Sheldrick, *SHELXL 97, Program for Crystal Structure Refinement*, University of Göttingen, Göttingen, 1997.
20 H. J. Lee, W. Cho and M. Oh, *CrystEngComm*, 2010, **12**, 3959.
21 S. Diring, S. Furukawa, Y. Takashima, T. Tsuruoka and S. Kitagawa, *Chem. Mater.*, 2010, **22**, 4531.
22 K. B. Wang, Z. R. Geng, Y. X. Yin, X. Y. Ma and Z. L. Wang, *CrystEngComm*, 2011, **13**, 5100.
23 D. S. Chowdhuri, A. Rana, M. Bera, E. Zangrando and S. Dalai, *Polyhedron*, 2009, **28**, 2131.
24 S. Wang, L. Zhang, G. Li, Q. Huo and Y. Liu, *CrystEngComm*, 2008, **10**, 1662.
25 S. Pramanik, C. Zheng, X. Zhang, T. J. Emge and J. Li, *J. Am. Chem. Soc.*, 2011, **133**, 4153.
26 H. Jung, D. Lee and K. Y. Jung, *J. Alloys Compd.*, 2005, **390**, 189.
27 Oshio, K. Kitamura, T. Shigeta, S. Horii, T. Matsuoka, S. Tanaka and H. Kobayashi, *J. Electrochem. Soc.*, 1999, **146**, 392.
28 Vallet-Regí, F. Balas and D. Arcos, *Angew. Chem., Int. Ed.*, 2007, **46**, 7548.
29 P. Lundberg, M. V. Walter, M. I. Montañez, D. Hult, A. Hult, A. Nyström and M. Malkoch, *Polym. Chem.*, 2011, **2**, 394.
30 D. B. Warheit, C. M. Sayes, K. L. Reed and K. A. Swain, *Pharmacol. Ther.*, 2008, **120**, 35.
31 J. Meletiadis, J. F. Meis, J. W. Mouton, J. P. Donnelly and P. E. Verweij, *J. Clin. Microbiol.*, 2000, **38**, 2949.
32 A. Tavman, I. Boz and A. S. Birteksöz, *Spectrochim. Acta, Part A*, 2010, **77**, 199.
33 B. Prathima, Y. S. Rao, S. A. Reddy, Y. P. Reddy and A. V. Reddy, *Spectrochim. Acta, Part A*, 2010, **77**, 248.
34 E. Viuelas-Zahnos, F. Luna-Giles, P. Torres-Garca and M. C. Fernndez-Caldern, *Eur. J. Med. Chem.*, 2011, **46**, 150.
35 H. F. A. El-Halim, M. M. Omar and G. G. Mohamed, *Spectrochim. Acta, Part A*, 2011, **78**, 36.